International Journal of Mining Science and Technology 33 (2023) 243–250

Contents lists available at ScienceDirect

International Journal of Mining Science and Technology

journal homepage: www.elsevier.com/locate/ijmst

# Experimental research on influence mechanism of loading rates on rock pressure stimulated currents

Min Li [a,b], Zhijun Lin [a], Shiliang Shi [a,*], Deming Wang [c], Yi Lu [a], He Li [a], Qing Ye [a], Xiaonan Zhang [a]

[a] School of Resource, Environment and Safety Engineering, Hunan University of Science and Technology, Xiangtan 411201, China
[b] State Key Laboratory of Coal Resources and Safe Mining, China University of Mining and Technology, Xuzhou 221116, China
[c] School of Safety Engineering, China University of Mining and Technology, Xuzhou 221116, China

ARTICLE INFO

*Article history:*
Received 13 April 2022
Received in revised form 30 June 2022
Accepted 27 December 2022
Available online 6 January 2023

*Keywords:*
Pressure stimulated current
Loading rate
Influence mechanism
Peak current

ABSTRACT

The study of pressure stimulated current (PSC) changes of rocks is significant to monitor dynamic disasters in mines and rock masses. The existing studies focus on change laws and mechanism of currents generated under the loading of rocks. An electrical and mechanics test system was established in this paper to explore the impacts of loading rates on PSCs. The results indicated that PSC curves of different rocks had different change laws under low/high loading rates. When the loading rate was relatively low, PSC curves firstly changed gently and then increased exponentially. Under high loading rates, PSC curves experienced the rapid increase stage, gentle increase stage and sudden change stage. The compressive strength could greatly affect the peak PSC in case of rock failure. The loading rate was a key factor in average PSC. Under low loading rates, the variations of PSCs conformed to the damage charge model of fracture mechanics, while they did not at the fracture moment. Under high loading rates, the PSCs at low stress didn't fit the model due to the stress impact effects. The experimental results could provide theoretical basis for the influence of loading rates on PSCs.



## 1. Introduction

Coal mining has gradually entered the stage of deep mining in China. Meanwhile, the coal and rock dynamic disasters such as rock burst and coal and gas outburst become increasingly serious and complex, which has strong impacts on efficient and safe production of coal mines [1,2]. Besides the direct hazards, they may easily trigger other tremendous accidents. Gas explosion occurs occasionally during the coal mining, due to a large amount of electric charge released along with the redistribution and fracture of roof rock stress [3–5]. The essential reason and monitoring mechanism of these dynamic disasters are that the roof rock produces freely moving charges when the stress changes [6,7]. Therefore, it is of great significance to study the current changes generated by stress stimulation of the rock to prevent coal mine roof dynamic disasters and the induced secondary disasters.

A large number of studies have proved that currents are formed by freely moving charges produced during the deformation process of rocks under loads. This kind of current is called the pressure stimulated current (PSC). The macroscopic laws and generating mechanism of PSCs have been studied in different types of rocks, such as marble, granite, sandstone and coal rock [8]. Stavrakas, Anastasiadis and etc. studied the change laws of currents generated in marble under the action of uniaxial compression. It is generally believed that these currents are generated during the initiation and propagation of cracks in the rock [9–11]. The most representative theory is moving charged dislocations (MCD) model, proposed by Slifkin and further improved by Vallianatos and Tzanis based on change laws of currents in different rocks under uniaxial compression [12–14]. In some experiments, PSCs will only be detected when the stress applied to the rock specimen exceeds a certain level [15,16]. While in other experiments, PSCs will be generated immediately when any significant stress is applied to the rock specimen [9,17,18]. When the stress is at a constant level, PSCs will attenuate and remain constant when it attenuates to a certain value. The reason for this difference is the different lithology and mechanical properties of rocks [19–21]. A large number of experimental results have indicated that the change of PSC values is closely related to mechanical properties of the tested rock samples [22–26].

The mechanical property parameters of rocks are not only related to the natural occurrence conditions such as rock types, mineral compositions and cementation types, but also closely

* Corresponding author.
*E-mail address:* sslhnust@yeah.net (S. Shi).

https://doi.org/10.1016/j.ijmst.2022.12.004
2095-2686/

related to the loading rates [27–29]. During the coal mining, the temporal and spatial changes of mining velocity and stress distribution will change the loading rate of the roof overburden, and thus PSC characteristics of roof rock will be changed, thereby affecting the stability prediction of the rock. The current research focuses on the change laws and mechanism of PSCs to reveal the generating mechanisms of earthquakes and coal mine dynamic disasters and provide theoretical basis for the prediction of earthquakes and volcanic eruption, and the rock mass instability monitoring. However, there are few studies on PSC changes of the rock masses with different lithology during the loading, and the influence mechanism is still unclear. Therefore, this paper constructed a rock electrical and mechanics test system, explored the variation law of PSCs of rock with different lithology, analyzed the mechanical effect of PSCs under different loading rates, and provided a theoretical basis for the mechanical influence mechanism of electrical effect during the process of rock failure.

## 2. Experimental methods

### 2.1. Experimental specimens

In this paper, the rocks with different lithologies were chosen as the research objects, including the granite (belonging to magmatic rocks) from Yantai, Shandong province, marble (belonging to metamorphic rocks) from Dali, Yunnan province, and sandstone (belonging to sedimentary rocks) from Renlou coal mine, Anhui Province. After obtaining bulk rock specimens, the rocks with high homogeneity and sound mechanical properties were selected and processed into cylinders of $\varphi$50 mm × 100 mm. The residual rock specimens were used for X-ray diffraction analysis (XRD) and SEM (scanning electron microscopy) analysis. As shown in Fig. 1, the granite is dominated by quartz, followed by amphibole and biotite. Marble mainly consists of dolomite, with a small amount of amphibole. The main composition of sandstone in Renlou deposit is quartz, followed by albite and a small amount of mica. In order to avoid stress concentration during the loading process, the upper and lower surfaces of each specimen were polished, and the surface roughness didn't exceed ±0.05 mm. After selecting a certain number of rock specimens, the specimens with larger differences were eliminated using the ultrasonic velocimeter. In order to achieve the drying effect and reduce the influence of polarization potential, the processed rock specimens were dried in a vacuum drying oven at 60 °C for 48 h to eliminate free water.

### 2.2. Experimental system and process

In this paper, a PSC test system was constructed for the failure of rock materials under uniaxial compression. It was used to measure the current, stress and strain changes over time during the compression deformation and failure process of granite, marble and sandstone. It was mainly composed of a uniaxial compression test system, PSC data acquisition system and a shielding and protection system. Fig. 2 shows the schematic diagram of the system.

In this paper, the electro-hydraulic universal testing machine MTS-C64.605 was used for the uniaxial compression testing to record the real-time changes of parameters such as force, load, strain and etc. Its computing system can record and calculate the stress and strain changes of rock specimens under loading, as shown in Fig. 2. The Keithley DMM6500 was used to acquire currents generated by the rock specimens from the loading process to the failure process. With high accuracy and large measuring range, it could directly collect the waveforms in the measurement range of 10 pA and 10 A, without using the separate instrument. As shown in Fig. 2, one end of the DMM was connected to the lower indenter through an alligator clip, and one end was grounded. The connecting wires were shielded cables and were not subjected to external electromagnetic interference. The indenter was made of stainless steel, whose deformation and resistance could be ignored. During the experiment, the rock specimens and the experimental system needed to be shielded and protected, so that the collected voltage data were true and effective. Besides, the 200 copper mesh was used to make a Faraday cage to cover the rock specimens and press blocks, thus isolating the interference of external electromagnetic signals. Meanwhile, the shielded cables could effectively reduce the noise. In order to prevent the debris generated during the loading and crushing process from splashing out and reduce unnecessary damages, a transparent protective cover was installed outside the testing machine.

### 2.3. Experimental process

The whole experiment was carried out according to the following steps:

(1) After the preparation of rock specimens, the ultrasonic velocity testing was conducted for the cylinders of $\varphi$50 mm × 100 mm to eliminate the specimens with larger differences. This could minimize the effects of the primary abnormal cracks or secondary cracks caused during the processing and ensure the experimental results.
(2) One end of the DMM6500 was connected to the lower indenter through an alligator clip, and the other end was grounded to test the currents generated by the rock specimens. The indenter was connected to the alligator clip through the copper tape. The resistance was zero on both sides of the copper tape. The data were stored by the computer. The resistance value of the insulating paper was effective, greater than 2.4 MΩ.
(3) After connecting the rock specimens and the experimental equipment, the MTS testing machine microcomputer system was started. Different loading rates were designed by programming. The force loading method was adopted in this experiment, and the loading method was the linear loading.

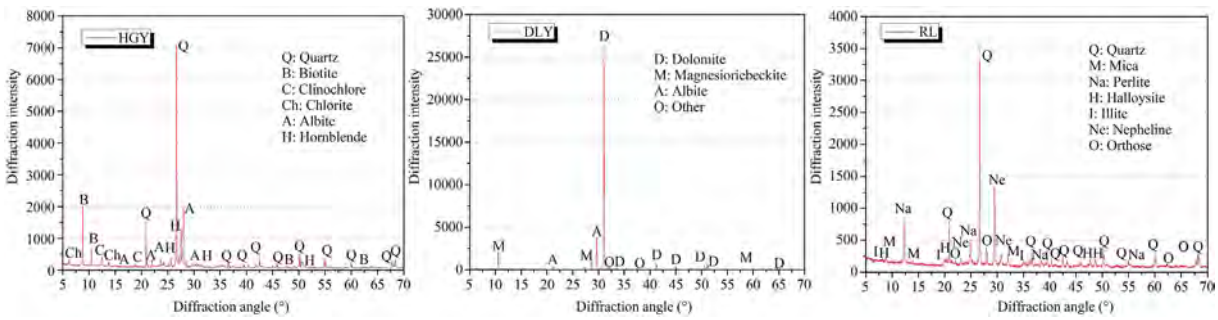


**Fig. 1.** Results of XRD.

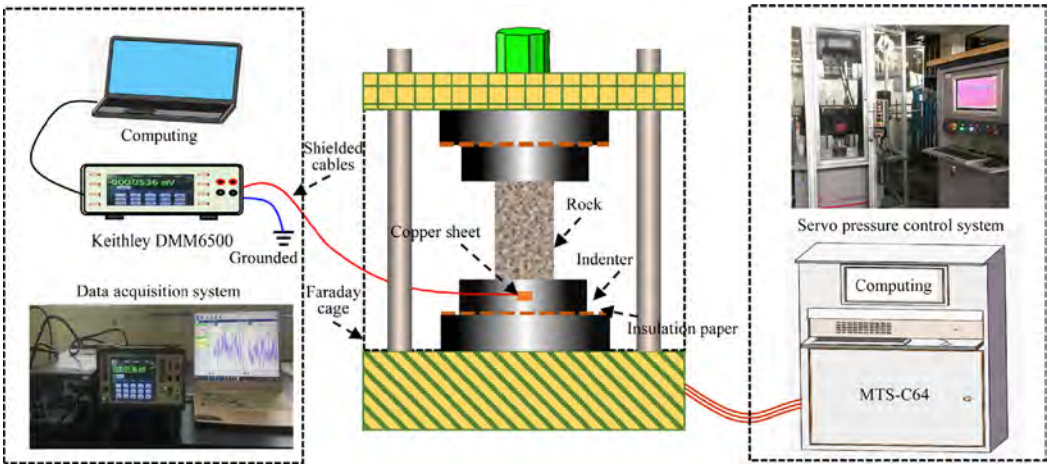


**Fig. 2.** Experiment system of PSC.

With the uniform loads, the linear loading method could be expressed as follows:

$$S = a \cdot t \tag{1}$$

where $S$ is the stress; $a$ the rate of the stress change, i.e. the loading rate; and $t$ the time.

When $t=S_{max}/a$, the rock specimen was broken, and $S_{max}$ represents the ultimate compressive strength of the rock specimen.

In this experiment, the loading rates were set as 0.5, 1, 5 and 10 kN/s. According to Kato [30], 0.5 and 1 kN/s belonged to the low loading rates, and 5 kN/s and 10 kN/s were high loading rates.

(4) The KickStart was started to choose proper sample rates, and other experimental parameters were set.
(5) After the preparation of each test system, the stress loading of the testing machine and the voltage test data collection were started at the same time.
(6) After the rock specimens were destroyed, the testing machine would automatically stop.

## 3. Results and analysis

### 3.1. PSC change laws under different loading rates

Different rock specimens were loaded by uniaxial loading, with the loading rates of 0.5, 1, 5 and 10 kN/s, respectively. The specimens of granite, marble and roof sandstone in Renlou coal mine were marked as HGY-0.5, HGY-1, HGY-5, HGY-10, DLY-0.5, DLY-1, DLY-5, DLY-10, RL-0.5, RL-1, RL-5 and RL-10, respectively. One end of the ammeter was grounded, so the current measurement value represented the flow of electric charge at one end of the rock specimen under loading. To facilitate the analysis of the change law, the absolute values of the current values were taken to analyze the magnitudes of the currents without analyzing the polarity changes.

Figs. 3–5 show the PSC change laws of specimens of granite, marble and roof sandstone under various loading rates. For the convenience of analysis, $s=S/S_{max}$ in the figure, where $S_{max}$ is the ultimate compressive strength and is a constant. Therefore, the change law of $S$ is the same as that of $s$. In Fig. 3, the PSC curves changed significantly with different loading rates under dry conditions. Obviously, the PSC curves showed different laws under different loading rates.

The PSC changes were small under low loading rates in the initial stage of loading. The current values remained constant at a low level or increased slowly, with low-frequency fluctuations. When the stress continued to increase and $t=t_d$, the current began to increase slightly. At this time, the corresponding stress level $S$ was $S_d$, and $s$ was $s_d$. When the stress continued to increase, the PSC increased exponentially until $t_f$, that is, the rock was completely damaged. At this point, $S=S_{max}$, and $s=1$. The stress reached the ultimate compressive strength of the rock. The peak $C_{peak}$ of PSC could be observed, which was consistent with the occurrence of stress mutation.

While under high loading rates, PSC curves could be divided into three stages in the whole loading process. At Stage I, PSC increased with the increase of the stress and reached the $C_{max}$ in a short time. Especially in Fig. 3d, there was a sudden increase in currents due to the stress impact in the initial stage of loading. The comparisons between Fig. 3c and d showed that the increase rates of the currents varied with the loading rates. As the stress increased, the current change entered Stage II. At this stage, the PSC changed slightly and the current values were basically the same or increased moderately. A downward trend could be observed in some areas. When the loading rate was 10 kN/s, the current value dropped slowly after the sudden increase in Stage I, and then increased slowly. When the stress continued, and $S=S_{max}$, PSC increased suddenly, quickly reached the peak for a short duration and then decreased. The time of peak occurrence was basically the same as that of stress mutation occurrence. After the peak current, the current value still maintained at a relatively high level, indicating that the granite could continue to discharge and form strong currents after experiencing the main failure. The results indicated that the PSC curves of the granite were different with various loading rates under the loading and failure process, and had good consistency with the stress. The current change could reflect the stress and failure state of the granite, but couldn't give advance warning. Similarly, PSC curves of marble and roof sandstone changed obviously under different loading rates in Figs. 4 and 5.

In summary, PSC curves of different rocks presented different change laws under low and high loading rates during the loading and failure process, with good consistency with the stress. The current change could reflect the loading and failure states of rocks.

The change of current could reflect the state of stress and destruction of the rock. At a lower loading rate, the PSCs first had a low level and a flat phase, and then an exponential growth phase. At high loading rates, PSCs went through three stages: the rapid growth stage, the gentle stage and the sudden change stage.

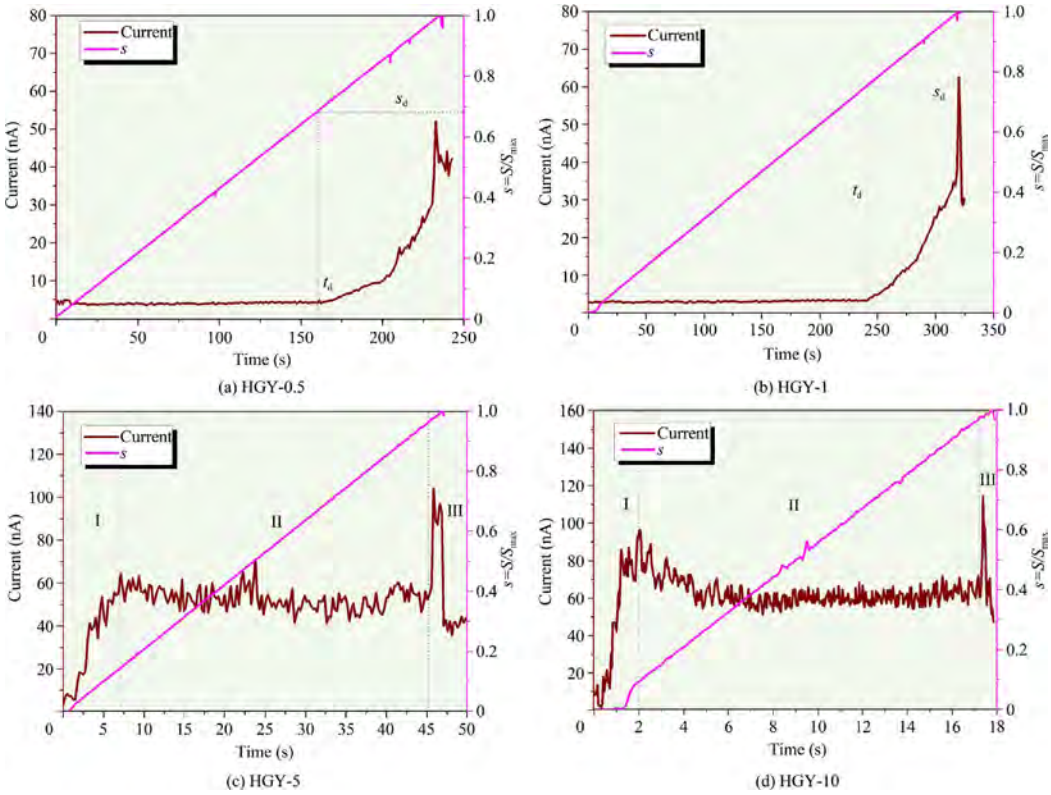


**Fig. 3.** PSC curves of granite under different loading rates.

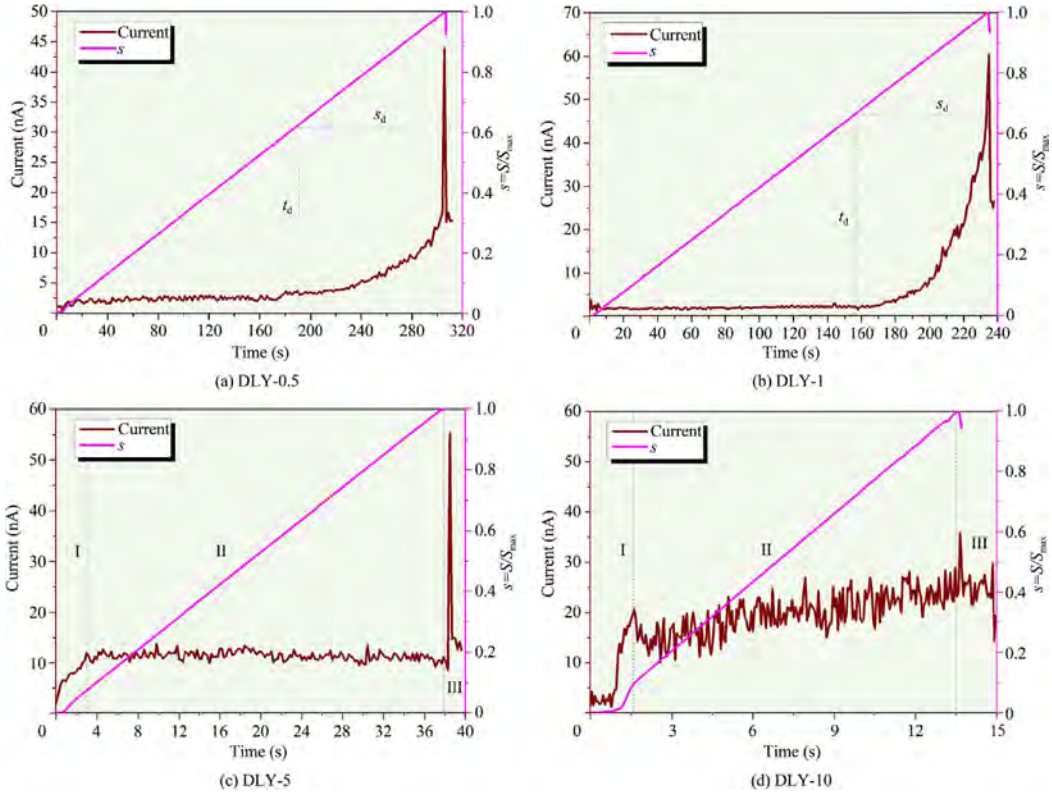


**Fig. 4.** PSC curves of marble under different loading rates.

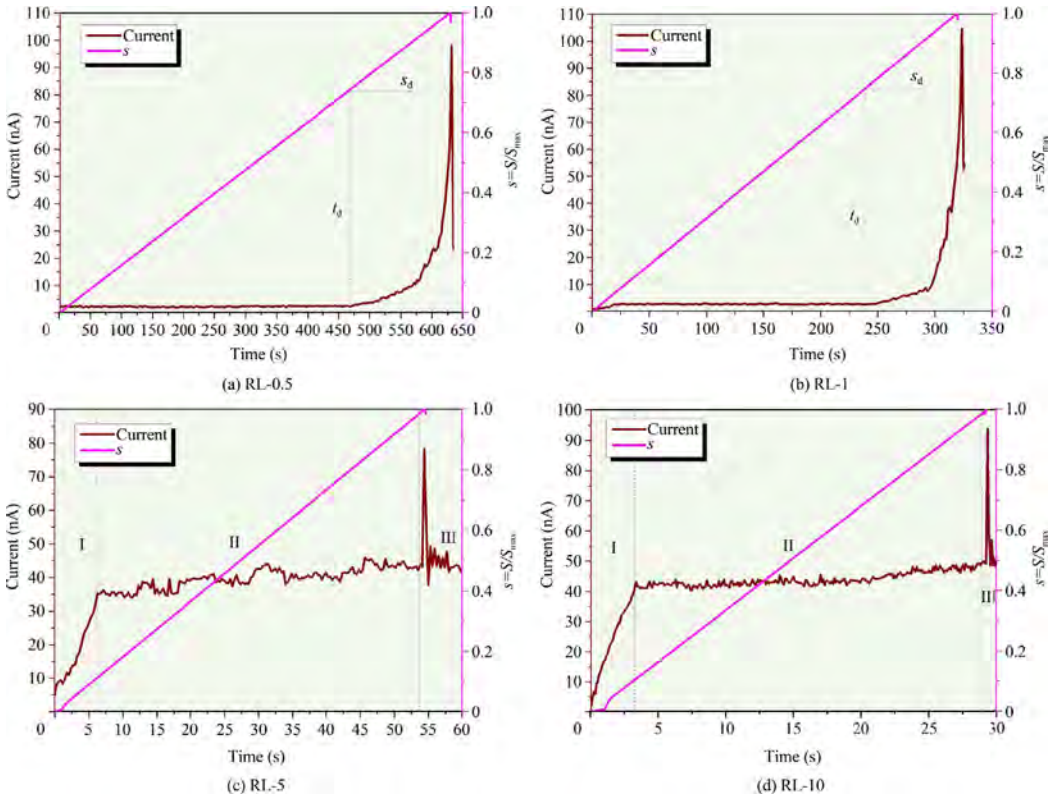


**Fig. 5.** PSC curves of sandstone under different loading rates.

### 3.2. Change characteristics of peak currents

In Section 2.1, the change laws of the PSC of a rock specimen were different under high and low loading rates. With the loading rates of 0.5 and 1 kN/s, $C_{peak}$ and $S_{max}$ of the specimen of the granite were 52.04 nA, 60.01 MPa and 62.6 nA, 80.05 MPa, respectively. When the loading rates were 5 and 10 kN/s, $C_{max}$ were 64.36 and 96.55 nA, respectively. The corresponding $C_{peak}$ and $S_{max}$ were 104.14 nA, 118.6 MPa and 97.67 nA, 88.22 MPa, respectively. For the specimen of the marble under the loading rates of 0.5 and 1 kN/s, $S_{max}$ and $C_{peak}$ were 77.73 MPa, 43.98 nA, and 118.14 MPa, 60.41 nA, respectively. When the loading rates were 5 and 10 kN/s, $C_{max}$ were 11.93 and 20.59 nA, respectively. $C_{peak}$ and $S_{max}$ were 55.26 nA, 95.35 MPa, and 35.87 nA, 67.28 MPa, respectively. For the specimen of the roof sandstone of the coal mine, when the loading rates were 0.5 and 1 kN/s, $C_{peak}$ and $S_{max}$ were 159.81 MPa, 84.15 nA, and 162.05 MPa, 104.61 nA. When the loading rates were 5 and 10 kN/s, $C_{max}$ were 35.41 and 43.2 nA, respectively. $C_{peak}$ and $S_{max}$ were 78.39 nA, 138.04 MPa, and 94.03 nA, 147.8 MPa.

Fig. 6 shows variations of peak currents of rock specimens under different loading rates. It could be seen that the peak currents were not consistent with the loading rates. They didn't increase with the increase of the loading rate, and there were no correlations between them. The loading rate couldn't affect the peak current, so it was not the decisive factor for the current formed at the moment of rock failure. Fig. 7 shows peak currents of rock specimens under different compressive strengths when fracture and unstability occurred. For the same rock specimen under failure, its peak currents increased with the increase of the compressive strength, without presenting linear relationship. The correlations between each rock specimen's compressive strength and peak currents were analyzed. The Pearson correlation coefficients of the granite, marble and roof sandstone of Renlou coal mine were 0.88, 0.967 and 0.954 in a 95% confidence interval.

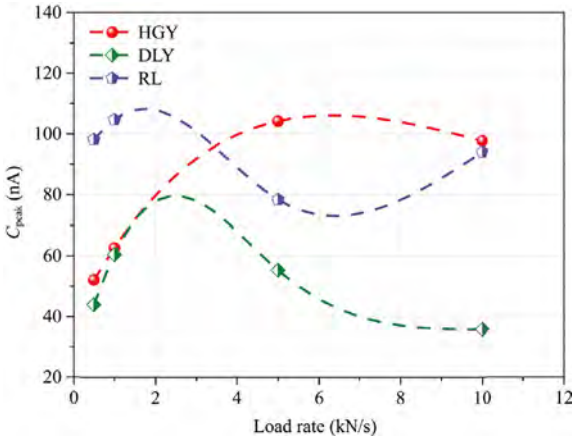


**Fig. 6.** Peak currents under different loading rates.

The values of $P$ were 0.12, 0.033 and 0.046, respectively. The $P$ value of granite was greater than 0.1, and other values were all less than 0.05, indicating that the compressive strength was significantly correlated with the peak current. Through the correlation analysis between the compressive strengths and peak currents of all rock specimens, the value of $P$ was 0.006, less than 0.01, presenting significant correlations. Therefore, the compressive strength was the key factor for generating peak currents in case of rock failure. In the process of uniaxial loading of the rock, micro-cracks occurred under various loading rates. After reaching the compressive strength, rock specimens subjected to larger compressive strengths generated more micro-cracks. When the rock specimen was fractured, a large number of micro-cracks penetrated instantly and formed stronger and abrupt peak current.

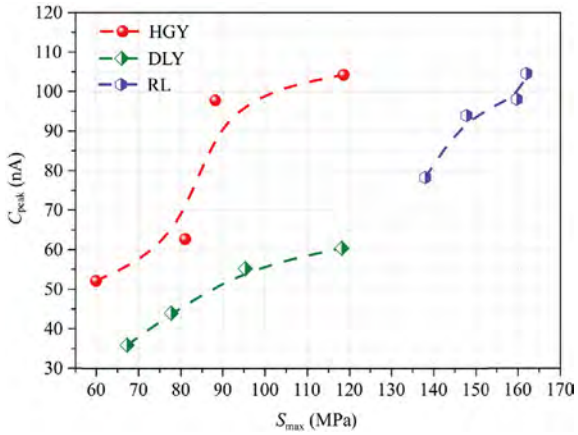


**Fig. 7.** Peak currents under different compressive strength.

Therefore, the compressive strength played a key role in generating peak currents in case of the rock specimen failure, which was a key factor affecting the occurrence of intense electromagnetic radiation and secondary disasters.

### 3.3. Change characteristics of average PSC

Lv et al. have evaluated the characteristics of charge generation on the surface of the rock through the accumulation of electrical signals [31]. However, the previous experimental results indicated that under different loading rates, the duration of rock specimens with different strengths varied from loading to failure. Meanwhile, due to instrument errors, the acquisition times were different under the same acquisition frequency. Besides, the rock specimens varied considerably, and there were large differences even for the same kind of specimens. Therefore, the cumulative electrical signals couldn't represent the electricity generation capacity of various rock specimens with different compressive strengths. Thus, the average current $C_A$ was proposed in this paper to evaluate the rock specimens' electricity generation capacity. It was expressed by the quotient of the cumulative current $C$ value and the cumulative acquisition times.

$$C_A = \frac{\sum C}{N} \tag{2}$$

where $N$ refers to the cumulative acquisition times during the loading process. $C_A$ of each specimen could be calculated.

Fig. 8 shows the change law of the average PSC of rock specimens under different loading rates. When the loading rate was low, the average PSC was relatively low. While the average PSC increased sharply under the high loading rates. On the whole, the average PSC increased as the loading rate increased, and the PSC was directly related with the loading rate from the loading to failure of the rock specimen. The correlation analysis results indicated that the Pearson correlation coefficients of the granite, marble and roof sandstone of Renlou coal mine were 0.949, 0.96 and 0.938, respectively, with a 95% confidence level. The values of $P$ were 0.051, 0.04 and 0.062, representing significant correlation, existing correlation and significant correlation. Therefore, the loading rate could determine the average PSC to some extent. Especially under the continuous loading conditions, the greater the loading rate, the higher the stress and the faster the crack propagation rate, the higher the electron energy level on the separation surface, and thus the stronger the PSCs. As the loading rate increased, more free charges would be generated per unit time, and higher PSC would be observed macroscopically.

Fig. 9 shows the average PSC in case of instability and failure of rock specimens under different compressive strength. It could be seen that there were no obvious relationships between the PSC and compressive strength. The greater the compressive strength of the rock specimen, the smaller the difference between the material mechanical parameters of the rock specimen unit. During the process of uniaxial loading, various micro-cracks occurred with different loading rates, while the micro-cracks rarely penetrated in rock specimens with relatively larger compressive strength. Fig. 10 shows the SEM experimental results of different rock specimens. Marble is a metamorphic rock whose microcrystal morphology is mostly irregular scaly and disorderly accumulation. It was composed mostly of dolomites and its compressive strength was large. There were large gray areas on the smooth specimen surface of granite and Renlou Mine roof sandstones, whose main mineral composition was feldspar. Meanwhile, there were large irregular, granular shiny white areas whose mineral composition was quartz. It could be seen that the quartz crystals of granite were more stereoscopic with larger and irregular particles. The quartz of sandstone was flaky grains with sedimentary rocks, and the particles were tightly combined with the cements. Both the granite and sandstone had extremely strong compressive strength, especially the roof sandstone of Renlou Mine. Weak surfaces were hard to be formed by the mirco-cracks around the crystal particles due to the cements, so the average generation ratezhi of electric charge was not affected by the strength. After reaching the compressive strength, the rock specimens with larger compressive strength generated. In case of failure, a large number of micro-cracks

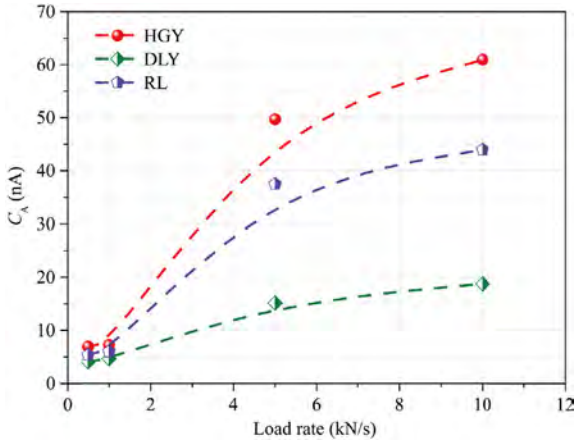


**Fig. 8.** Average PSC under different loading rates.

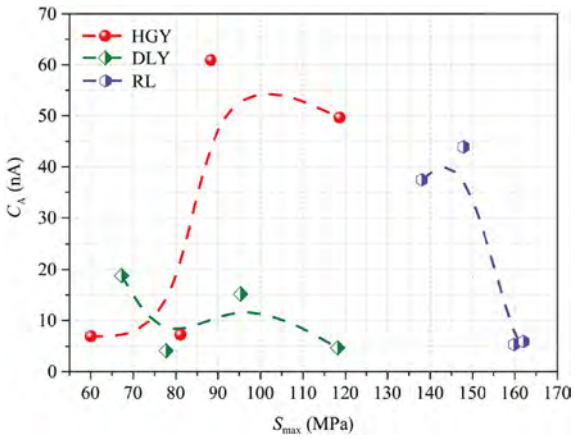


**Fig. 9.** Average PSC under different compressive strengths.

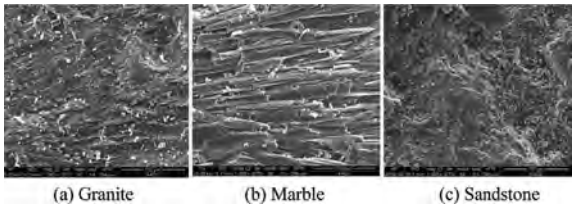


**Fig. 10.** SEM results of different rock samples.

penetrated instantaneously and thus formed stronger and sudden peak PSC. Therefore, the compressive strength was a key factor for the peak PSC, and the loading rate could determine the average PSC during the loading process of the rock specimen.

## 4. Influence mechanism of loading rates on PSCs

The fracture of heterogeneous rock masses is usually a complex nonlinear process, which involves highly complex interactions across multiple time/length scales under non-equilibrium conditions. During the deformation process, PSCs occurred under various mechanisms when rock specimens were subjected to external stresses. These mechanisms were related to crack initiation and propagation processes. The fracture and stress induced effects could be regarded as irreversible kinetic results of disordered systems resulting from scale-invariant long-term interactions. The stress $S$ of the rock specimen was a function of the strain $\varepsilon$ in the linear-elastic range, which could be expressed as Eq. (3).

$$S = \mathrm{Y}_0 \cdot \varepsilon \tag{3}$$

where $Y_0$ is the constant Young's modulus of undamaged materials in the elastic range. When the stress exceeds the elastic range, micro-cracks will occur. For a given $S$, the strain $\varepsilon$ shall be larger than the value calculated by the Eq. (3). Therefore, Eq. (4) could be obtained.

$$S = \mathrm{Y}_\mathrm{e} \cdot \varepsilon \tag{4}$$

where $Y_e$ is the effective elastic modulus, and is no longer constant. It decreased gradually with the increase of stress in the plastic range. In order to present the process, the damage parameter $D$ was introduced and expressed by Eq. (5).

$$\mathrm{Y}_\mathrm{e} = \mathrm{Y}_0(1 - D) \tag{5}$$

The damage parameter could quantitatively describe the deviation from linear elastic fracture, so it could represent the rate of micro-crack generation, within the range of 0 to 1. When $D$ was 0, the rock specimen was in the linear-elastic stage, which could be expressed by Eq. (3). When $D$ was 1, the rock specimen failure occurred. According to Vallianatos and Tzanis's theoretical model of current generation due to stress both in piezoelectric and non-piezoelectric rocks, the pressure stimulated current $I$ was proportional to the strain rated $d\varepsilon/dt$. Thus, if $Y$=$Y_0$ (a constant), then

$$I \propto \frac{\mathrm{d}\varepsilon}{\mathrm{d}t} \tag{6}$$

If $Y$=$Y_e$, according to Eqs. (3) and (4), Eq. (7) could be obtained.

$$I \propto \frac{1}{\mathrm{Y}_\mathrm{e}}\frac{\mathrm{d}\varepsilon}{\mathrm{d}t} \propto \frac{1}{1-D}\frac{\mathrm{d}\varepsilon}{\mathrm{d}t} \tag{7}$$

To facilitate the analysis, the graph was drawn with $s$ as the $y$-axis, and $\varepsilon$ as the $x$-axis. Fig. 11 shows the stress–strain curves of the granite, marble and sandstone with the loading rate of 1 kN/s. When $s$ was less than 0.3, their strain change rate was relatively large, and the specimens were at the stage of compaction. When $s$ was larger than 0.3, the strain curves increased linearly, and the rock specimens were at the linear-elastic stage. As the stress continued to increase, the stress-strain curves began to deviate from the straight line. At this point, $s$=$s_d$. It was remarkable that when the normal stress ($s$=0.065) exceeded the limit value, the rock specimens were beyond the linear-elastic range. The Young's modulus decreased as the stress increased. Therefore, when $s$ was between 0.6 and 0.75, regardless of rock types, PSC began to increase. That is, the transient currents occurred, which was consistent with the results obtained by Eq. (7) and the current change law in Section 3.1. d$S$/d$t$ was constant, but the change of PSC was caused by the changes of Young's modulus.

To sum up, no obvious PSCs were observed under low loading rates, with d$S$/d$t$=a (a constant) and Eq. (3) was effective ($s$<$s_d$). Micro-cracks began to occur when the stress exceeded the elastic limit (Eq. (4)). They continued to propagate and develop as the stress increased. Finally, the non-elastic deformation occurred and the transient and enhanced PSC could be observed. The results in Fig. 11 showed that under low loading rates, the currents conformed to the damage model of the fracture mechanics, while they did not at the moment of rupture. Under high loading rates, PSCs could be detected even though external stresses were applied to the rock specimens in the linear range. At this point, the original cracks of the rock closed rapidly due to the impact effects of the loading rate. Meanwhile, new cracks occurred and PSCs were also generated.

## 5. Conclusions

In this paper, the uniaxial compression PSC test system was established to explore the influences of the loading rates on PSCs of rocks. The conclusions were given as follows:

(1) PSC curves varied for different rock specimens under low/high loading rates, which were highly consistent with the stresses. When the loading rate was relatively low, the PSC

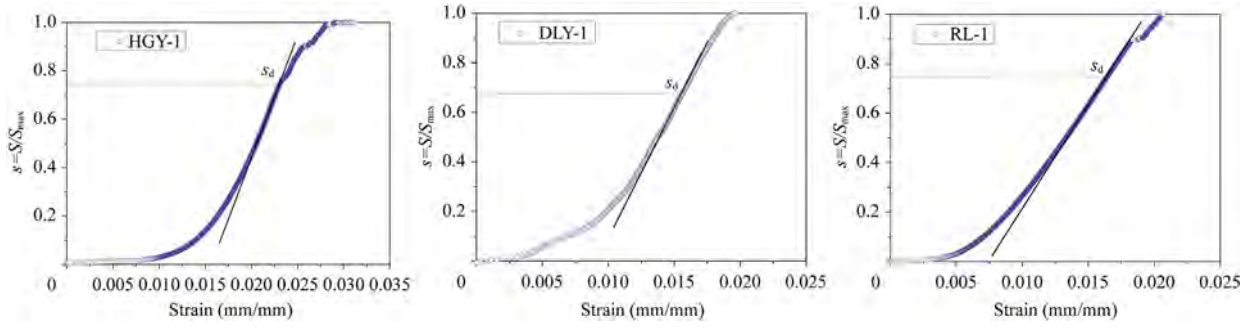


**Fig. 11.** Stress–strain curves of the rock samples.

was firstly small and gentle, and then increased exponentially. In case of high loading rates, PSC experienced the rapid increase stage, gentle stage and sudden change stage.

(2) Pearson correlation coefficients of the granite, marble and sandstone were 0.88, 0.967 and 0.954 in a 95% confidence interval of compressive strength and peak current. The granite's $P$ value was greater than 0.1, while marble and sandstone's $P$ values were less than 0.05, indicating that the compressive strength played a key role in generating peak currents in case of rock failure.

(3) The loading rate could determine the average PSC of the rock. Under the continuous loading, the greater the loading rate, the faster the growth rate of the cracks, the higher the electronic level on the separation surface, and the easier the generation of free charges. The loading rate could determine the generation rate of the micro-cracks of the rock specimen, so the faster the generation of the free charges, the larger the currents.

(4) Under low loading rates, when $dS/dt$=a(a constant), no significant transient PSCs could be observed. When the stress exceeded the elastic limit, micro-cracks began to occur. As the cracks propagated and expanded, the transient and enhanced PSCs could be detected. While under high loading rates, due to the impact effects of the loading rates, even if stresses were applied to the rock specimen in the linear range, the increased PSCs could also be detected.

## Acknowledgements

This project was funded by the Research Fund of the State Key Laboratory of Coal Resources and Safe Mining, China University of Mining and Technology (No. SKLCRSM22KF011), the National Natural Science Foundation of China (Nos. 52130411, 52104191, 51974120, and 51904103), the Natural Science Foundation of Hunan Province (No. 2021JJ40204), and the Science and Technology Innovation Program of Hunan Province (No. 2020RC3047).

## References

[1] He S, Lu Y, Li M. Probabilistic risk analysis for coal mine gas overrun based on FAHP and BN: A case study. Environ Sci Pollut Res 2022;29(19):28458–68.
[2] Shi H, Song L, Zhang H, Chen W, Lin H, Li D, Wang G, Zhao H. Experimental and numerical studies on progressive debonding of grouted rock bolts. Int J Min Sci Technol 2022;32(1):63–74.
[3] Li M, Wang HT, Wang DM, Shao ZL, He S. Risk assessment of gas explosion in coal mines based on fuzzy AHP and Bayesian network. Process Saf Environ Prot 2020;135:207–18.
[4] Brady BT, Rowell GA. Laboratory investigation of the electrodynamics of rock fracture. Nature 1986;321(6069):488–92.
[5] Li M, Lv H, Lu Y, Wang DM, Shi SL, Li RQ. Instantaneous discharge characteristics and its methane ignition mechanism of coal mine rock damage. Environ Sci Pollut Res 2022:1–12.
[6] Li M, Wang DM, Shao ZL. Experimental study on changes of pore structure and mechanical properties of sandstone after high-temperature treatment using nuclear magnetic resonance. Eng Geol 2020;275:105739.
[7] Meng T, Yue Y, Ma J, Jiao B, Niu H, Wen L, Yongbin X. Use of DC voltage fluctuation method to investigate real-time Mode I and Mode II subcritical crack growth behavior in gypsum rock. Eng Fract Mech 2020;234:107104.
[8] Qiu LM, Liu ZT, Wang EY, He XQ, Feng JJ, Li BL. Early-warning of rock burst in coal mine by low-frequency electromagnetic radiation. Eng Geol 2020;279:105755.
[9] Stavrakas I, Triantis D, Agioutantis Z, Maurigiannakis S, Saltas V, Vallianatos F, Clarke M. Pressure stimulated currents in rocks and their correlation with mechanical properties. Nat Hazards Earth Syst Sci 2004;4(4):563–7.
[10] Ren B, Yuan L, Zhou G, Li SL, Meng QZ, Wang K, Jiang BY, Yu GF. Effectiveness of coal mine dust control: A new technique for preparation and efficacy of self-adaptive microcapsule suppressant. Int J Min Sci Technol 2022;32(6):1181–96.
[11] Li H, Tian L, Huang B, Lu J, Shi S, Lu Y, Huang F, Liu Y, Zhu X. Experimental study on coal damage subjected to microwave heating. Rock Mech Rock Eng 2020;53(12):5631–40.
[12] Slifkin L. Seismic electric signals from displacement of charged dislocations. Tectonophysics 1993;224(1–3):149–52.
[13] Vallianatos F, Triantis D. Scaling in pressure stimulated currents related with rock fracture. Phys A Stat Mech Appl 2008;387(19–20):4940–6.
[14] Tzanis A, Vallianatos F, Gruszow S. Identification and discrimination of transient electrical earthquake precursors: Fact, fiction and some possibilities. Phys Earth Planet Interiors 2000;121(3–4):223–48.
[15] Zhou ZL, Cai X, Li XB, Cao WZ, Du XM. Dynamic response and energy evolution of sandstone under coupled static–dynamic compression: Insights from experimental study into deep rock engineering applications. Rock Mech Rock Eng 2020;53(3):1305–31.
[16] Cai X, Zhou ZL, Zang HZ, Song ZY. Water saturation effects on dynamic behavior and microstructure damage of sandstone: Phenomena and mechanisms. Eng Geol 2020;276:105760.
[17] Anastasiadis C, Triantis D, Stavrakas I, Vallianatos F. Pressure Stimulated Currents (PSC) in marble samples. Ann Geophys 2004;47(1).
[18] Li H, Xu C, Ni G, Lu J, Lu Y, Shi S, Li M, Ye Q. Spectroscopic (FTIR, 1H NMR) and SEM investigation of physicochemical structure changes of coal subjected to microwave-assisted oxidant stimulation. Fuel 2022;317:123473.
[19] Wang EY, Chen P, Liu ZT, Liu YJ, Li ZH, Li XL. Fine detection technology of gas outburst area based on direct current method in Zhuxianzhuang Coal Mine. China Saf Sci 2019;115:12–8.
[20] Wang EY, Jia HL, Song DZ, Li N, Qian WH. Use of ultra-low-frequency electromagnetic emission to monitor stress and failure in coal mines. Int J Rock Mech Min Sci 2014;70:16–25.
[21] Wang EY, He XQ, Wei JP, Nie BS, Song DZ. Electromagnetic emission graded warning model and its applications against coal rock dynamic collapses. Int J Rock Mech Min Sci 2011;48(4):556–64.
[22] Li M, Wang HT, Wang DM, Shao ZL. Experimental study on characteristics of surface potential and current induced by stress on coal mine sandstone roof. Eng Geol 2020;266:105468.
[23] Archer JW, Dobbs MR, Aydin A, Reeves HJ, Prance RJ. Measurement and correlation of acoustic emissions and pressure stimulated voltages in rock using an electric potential sensor. Int J Rock Mech Min Sci 2016;89:26–33.
[24] Freund FT, Freund MM. Paradox of peroxy defects and positive holes in rocks. Part I: Effect of temperature. J Asian Earth Sci 2015;114:373–83.
[25] Vallianatos F, Triantis D. A non-extensive view of the pressure stimulated current relaxation during repeated abrupt uniaxial load-unload in rock samples. EPL Europhys Lett 2013;104(6):68002.
[26] Freund FT, Takeuchi A, Lau BWS. Electric currents streaming out of stressed igneous rocks-A step towards understanding pre-earthquake low frequency EM emissions. Phys Chem Earth Parts A/B/C 2006;31(4–9):389–96.
[27] Li ZH, Niu Y, Wang EY, He M. Study on electrical potential inversion imaging of abnormal stress in mining coal seam. Environ Earth Sci 2019;78(8):1–14.
[28] Liu YJ, Li XL, Li ZH, Chen P, Yang T. Experimental study of the surface potential characteristics of coal containing gas under different loading modes (uniaxial, cyclic and graded). Eng Geol 2019;249:102–11.
[29] Li D, Wang E, Li Z, Jia H, Wang D, Kong X, Wang X, Wang X, Ali M. A causal mechanism for anomalous electromagnetic radiations from coal and rock failure. Geophysics 2018;83(6):E423–34.
[30] Kato M, Mitsui Y, Yanagidani T. Photographic evidence of luminescence during faulting in granite. Earth Planet Sp 2010;62(5):489–93.
[31] Lv XF, Pan YS, Xiao XC, Wang AW. Barrier formation of micro-crack interface and piezoelectric effect in coal and rock masses. Int J Rock Mech Min Sci 2013;64:1–5.